AN EXPERIMENTAL STUDY ON TURBULENT SWIRLING WATER FLOW WITH IMMISCIBLE DROPLETS

Takuro Kouda
Division of Mechanical and System Engineering
Graduate School of Engineering and Design, Kyoto Institute of Technology,
Matsugasaki, Kyoto 606-8585, Japan
taku04@kit.ac.jp

Yoshimichi Hagiwara
Department of Mechanical and System Engineering
Kyoto Institute of Technology,
Matsugasaki, Kyoto 606-8585, Japan
yoshi@kit.ac.jp

ABSTRACT

We have carried out measurements of the flow field of turbulent swirling water flow with low-density immiscible oil droplets in a horizontal pipe. The swirl is obtained with a stationary impeller inside the pipe. The flow is visualized with tracer particles and the images of visualized flow are captured from the side and downstream-end of the pipe with video cameras. The instantaneous velocity field is measured from the captured images with the particle tracking velocimetry method. The experimental results show that the low-density droplets have relative motion to the ambient water due to the buoyancy force and lift force. The periodic pulsative wake flow of the droplets causes the increase in the turbulence intensity.

INTRODUCTION

There has been a sense of growing crisis in relation to global warming. Various promising methods have been proposed to reduce global warming. One of them is the recovery of waste heat. The total amount of waste heat in warm water from factories, hotels and houses is not negligible, though the energy density of the waste heat is low at each site. Development of a highly efficient method of heat transfer is required for the recovery of waste heat.

Direct-contact heat transfer between the water flow (continuous-phase flow) and immiscible droplets (dispersed phase) meets the requirement because of the mixing effect of the droplets and the increase in the heat transfer surface by introducing many small droplets. Therefore, this direct-contact heat transfer has been studied widely recently. Lee (1987) measured the overall heat transfer coefficient and the size distribution of droplets. Jacobs and Golafshani (1989) showed that the circulation inside the immiscible droplets enhanced heat transfer. Kaviany (1994) summarized the interaction between an immiscible droplet and its surrounding flow. Mitrovic and Stephan (1996) derived equations for mean temperatures for the direct contact heat exchange without evaporation. Inaba et al. (1998) obtained empirical equations for inter-phase heat transfer and the size distribution of droplets injected into the water flow. In these studies, the droplets moved in the central regions of the flows because the heat of one phase could be transferred efficiently to the other phase in these regions.

In the case of small-scale distributed heat exchangers for the factories, hotels and houses, flows with immiscible droplets in passages in vertical and horizontal directions should be considered. Our group showed that the immiscible droplets of low specific weight in turbulent downward water flow in a duct approached the duct wall far from the injection nozzle of droplets (Hagiwara et al., 2005). We also indicated that the immiscible droplets (of high specific weight injected in turbulent upward water flow in a pipe) approached the pipe wall eventually (Hagiwara et al, 2003). These wallward motions of the droplets are due to the lift force acting on the droplets. In the case of horizontal flows, the droplets, whose density is different from that of water, move towards the wall due to buoyancy force or gravitational force. The attenuation of these wallward motions of droplets, or more generally the control of droplets motions in the different types of flow, is highly desirable to maintain efficient heat transfer between the phases.

We have considered that adding rotation to the main flow is effective for the attenuation of the wallward motion of the droplets. Magaud et al., (2003) carried out their experimental and theoretical study on swirling water flow with bubbles in a vertical pipe. However, their results are not available to predict the flow characteristics of the horizontal turbulent swirling flow with immiscible droplets. Thus, we carried out an experiment on the turbulent swirling water flow with silicon-oil droplets in a horizontal pipe and discussed the forces acting on the droplets and the turbulence modification due to the droplets (Kouda and Hagiwara, 2005).

In the present study, we measure the droplets motions and flow turbulence in the case of a stronger swirl than that in our previous study and discuss the force balance acting on the droplets and turbulence modification due to the droplets.

APPARATUS

Test loop

The apparatus is shown schematically in Fig. 1. This apparatus is the same as that in our previous study (Kouda and Hagiwara, 2005). The test loop consisted of an upstream chamber, a contraction nozzle, a horizontal pipe made of acrylic resin, an elbow with a window, a downstream chamber, a pump and connecting tubes. The flow rate of water was controlled by an inverter for the pump.

The inner diameter of the pipe, D, was 50 mm and the total length was 3050 mm (= 61D). A tripping wire was attached to the inner surface at the inlet of the pipe in order to promote turbulence. The Reynolds number based on D, the bulk mean velocity V_m and the kinematic viscosity ν, $Re_D = V_m D/\nu$, was 3.6×10^3.

Impeller

The swirl was obtained with a stationary impeller inside the pipe. The impeller was located at 2110 mm (= 42.2D) from the inlet of the horizontal pipe where the mean velocity field was developed. Figure 2 shows the detail of the impeller. The diameter of the boss for the blade of the impeller was 20 mm. The origin of the coordinates was at the center of the impeller. The x, y and z axes were positioned in a horizontal direction, a vertical direction and a downstream direction, respectively. The test section was allocated in the region of $115 < z < 715$ mm ($2.3D < z < 14.3D$).

The swirl number defined by the following equation (Kitoh, 1991) was used to estimate the effect of swirl on the main flow at the cross section:

$$Sw = \frac{2\pi \int_0^{D/2} V_\theta V_z r^2 dr}{\pi (D/2)^3 V_m^2}, \tag{1}$$

where V_θ is the time-averaged azimuthal velocity, V_z is the time-averaged axial velocity, $r = \sqrt{x^2 + y^2}$, is the radial coordinate. This swirl number is the ratio of the momentum due to the swirl in a specific cross section and the bulk mean momentum transported downstream. The swirl number at the test section was 1.04.

Immiscible Droplets

Silicon oil (KF995, Shin-Etsu Chemical Co., Ltd,) was adopted for the fluid of the immiscible droplets. The physical properties of these oils are shown in Table 1.

The silicon oils were injected from four fine stainless-steel tubes, whose inner diameter was 0.8 mm, simultaneously (See Fig. 2). The droplets were formed at the outlets of the tubes. These outlets were located at (0.25D, 0, 2.4D), (0, 0.25D, 2.4D), (-0.25D, 0, 2.4D) and (0, -0.25D, 2.4D). Each tube was connected with a syringe, and the syringes were pushed with a motor. The ratio of the total volumetric flow rate of oil to that of main water flow was 0.0020. The oil droplets were collected at the exit of the downstream chamber.

The Stokes number defined by the following equation was introduced for the purpose of analyzing the droplet motion:

$$St = \frac{\tau_d}{\tau_f} = \frac{2\rho_d + \rho}{36\mu} d^2 \Big/ \frac{D}{V_{\theta \max}}, \tag{2}$$

where τ_d is the characteristic time of a droplet, τ_f is the characteristic time of the swirl, ρ_d is the droplet density, ρ is the water density, μ is the water viscosity, d is the droplet equivalent diameter and $V_{\theta\max}$ is the maximum of the time-averaged azimuthal velocity. τ_d was estimated from the study carried out by Tanaka et al. (2002). Since $V_{\theta\max}$ is constant, the Stokes number depends only on the droplet diameter.

FLOW VISUALIZATION

The flow was visualized with the fluorescent tracer particles, which was made by adsorbing Rhodamine B to the particles for an ion-exchange process. The specific weight of the particle was 1.02. The diameter of these particles was in the range of 0.053 — 0.075 mm. Judging from the pixel ranges of the cameras mentioned below, these particles were detected by at least four pixels, which is appropriate for the particle tracking velocimetry (hereafter called PTV). Furthermore, the diameter was estimated to be approximately 0.16 — 0.38 times larger than the Kolmogorov length scale, l_K, calculated by the following equation:

$$l_\kappa = \left(\nu^3/\varepsilon\right)^{1/4} = \nu/\left(\varepsilon^{+1/4} v_\tau\right), \tag{3}$$

where ε is the dissipation rate of turbulent kinetic energy, ε^+ is its non-dimensional form and v_τ is the friction velocity. v_τ was calculated from the mean-wall shear stress, which was estimated from the mean velocity distributions in the axial and the azimuthal directions. The value of ε^+ was in the range of 0.02 — 0.16 depending on the distance from the pipe axis according to the numerical result obtained by Satake and Kunugi (1998).

We examined how much the particles follow sinusoidal fluid motion based on the result obtained by Hjelmfelt, Jr and Mockros (1966). The upper limit of the frequency, beyond which the particles cannot respond to the fluid motion completely, was estimated to be approximately 133 Hz, which was higher than the image capturing frequency mentioned below. Therefore, the particle was appropriate for the visualization of the water flow.

IMAGE CAPTURING

The outside of the pipe in the test section was covered with transparent plates as shown in Fig. 3. The gap between these plates and the outer surface of the pipe was filled with water in order to reduce the deformation of the image through the pipe wall.

Green light of Nd: YVO_4 laser was used as light source. The laser light was divided into two lines by a half mirror and then each line was expanded by using cylindrical lenses to obtain laser light sheet. When the velocity on a cross section (an (x, y)-plane) was measured, the light sheet illuminated the whole cross section through the rectangular box from above and below (See Fig. 3(a)). The width and thickness of the light sheet were 70 mm and 10 mm, respectively.

We added Rhodamine B to the water flow in order to highlight the phase interface because the dye does not dissolve in the silicon oils. The concentration of the dye was so low that the fluorescence intensity from the dye was much weaker than that from the tracer particles.

Fluorescence from the tracer particles and the dye in the water flow were captured by a progressive-scan CCD video camera (Basler, A202k) with an optical filter located at the downstream end of the pipe. The image-capturing condition is summarized in Table 2. The captured images were directly recorded into a personal computer through a frame grabber.

When the velocity on a vertical plane parallel to the axis (an (y, z)-plane) was measured, the lenses were rotated 90 degrees (See Fig. 3(b)). The width and thickness of the light sheet was 10 mm and 5 mm, respectively.

We adopted the shadow image technique (SIT) to obtain the phase interface. A blue LED array was allocated beside the pipe as a backlight for SIT. Fluorescence from the tracer particles and the LED backlight were captured by a color CMOS camera (Silicon video 9M001C) located at the other side of the pipe. The image-capturing condition is shown in Table 2. The captured images were directly recorded into a personal computer through a frame grabber.

IMAGE PROCESSING

Preprocessing

The particle mask correlation method developed by Etoh et al. (1999) was used for the digital images in the preprocessing. In this method, the Gaussian distribution of brightness was assumed for the image of each particle. For example, in the case of images on the (x, y)-plane, this distribution, $f(x, y)$, was given by the following equation:

$$f(x,y) = \exp\left\{\frac{-(x-x_0)^2-(y-y_0)^2}{(d_p/2)^2}\right\}, \quad (4)$$

where (x_0, y_0) is the position of the center of the particle. The distribution was used for the standard template. d_p was determined as equal to 4.0 × (pixel size) from the images. We removed weak scattered light from small particles on the images with this template.

The cross-correlation coefficient, $R_{fh}(x_i, y_j)$, was calculated between the template and the distribution of brightness in a small local area of $n \times n$ pixels^2 with a particle, h:

$$R_{fh}(x_i,y_j) = \frac{\sum_i^n\sum_j^n\left[f(x_i,y_j)-f_m\right]\cdot\left[h(x_i+dx,y_j+dy)-h_m\right]}{\sqrt{\sum_i^n\sum_j^n\left[f(x_i,y_j)-f_m\right]^2\cdot\sum_i^n\sum_j^n\left[h(x_i+dx,y_j+dy)-h_m\right]^2}}, \quad (5)$$

where h_m is the mean value of the brightness over the area, f_m is the mean value of the brightness over the $n \times n$ pixels^2 for the template, dx and dy are the displacements from the coordinate (x, y). n was set equal to 4 in the present study. If the coefficient takes a higher value than 0.7 (Okamoto et al., 2002) at a specific location, the center of the particle was considered to be at the apex of the Gaussian distribution. The same procedure was carried out in the case of (x, z)-planes.

Velocity Gradient Tensor Method

The PTV technique based on the velocity gradient tensor method developed by Ishikawa et al. (2000) was applied for obtaining velocity vectors from the preprocessed images. In this method, the matrix including the velocity gradient tensor was calculated for pairs of neighboring particles in a specific region around a particle. Then, the sum of the square of the errors was evaluated. This procedure was iterated for all the candidate particles until the sum took its minimum value. This method has the advantage of accurately reproducing velocity fields with strong deformation.

The velocities of the tracer particles were redistributed to the grid points of 32 × 32 in the x and y directions on the (x, y)-plane. The velocity of a particle was simply shifted to the nearest grid point in the redistribution procedure. The velocities of the particles were redistributed to the grid points of 32 × 1 in the y and z directions on the (y, z)-plane.

The uncertainty of the velocity was analyzed. The uncertainty due to the present method was estimated to be 1.0 mm/s for the maximum value of the azimuthal mean velocity of 74 mm/s on the (x, y)-plane. The uncertainty was estimated to be 2.3 mm/s for the maximum value of the axial mean velocity of 118 mm/s on the (y, z)-plane. These show that the measured velocity was accurate.

RESULTS AND DISCUSSION

Mean Velocities in the Azimuthal and Radial Directions

Figures 4(a) and 4(b) depict the profiles of azimuthal mean velocity, V_θ, along the horizontal and vertical axes in the case without the droplets, respectively. This velocity is found to increase almost linearly from zero near the axis with the absolute values of x and y in the regions of $-0.6 < 2x/D < 0.56$ and $-0.56 < 2y/D < 0.5$. This shows that the velocity field in the central region of $2r/D < 0.5$ is similar to that of a forced vortex. $V_{\theta\max}$ in Eq. (2) was determined from the profiles. Not that $V_{\theta\max}$ in the present study is approximately 1.9 times higher than that in our previous study. This shows that the swirl in the present study is stronger than that in the previous study.

The profiles of radial mean velocity, V_r, along the horizontal and vertical axes are also shown in Figs. 4(a) and (b). V_r takes slightly positive values in the regions of $-0.70 < 2x/D < 0$ and $-0.30 < 2y/D < 0$, and takes slightly negative values in the regions of $0 < 2x/D < 1$ and $0 < 2y/D < 1$. This shows that weak motion gathering into the pipe axis was superimposed on the swirl motion of the fluid. This is due to the wake flow of the boss of the impeller mentioned below. Therefore, the water in the test section has a spiral motion.

Detection Numbers of Droplets

Figure 5 indicates the total number of frames N, in which the droplets appeared, for the vertical plane of $x = 0$ at around $z/D = 3.4$. Thirty two slots whose width was $0.0313D$ were defined in the y direction, and the number for each slot was counted when the center of the droplet was in the slot. The

numbers take more than half their maximum value in the region of $-0.32 < 2y/D < 0.48$ except for $2y/D = 0.17$. That is, many droplets were transported in the central region. This is clearly different from the result obtained in our previous study in which many droplets were transported in the second quadrant region on the (x, y)-plane. This is because the radial coordinate of V_0, whose downward component balances with the upward velocity due to the buoyancy force, is closer to the axis than that of our previous study in the case of weak swirl. In this sense, the strong swirl is effective in concentrating the low-density droplets into the central region.

Diameter of Droplets

Figure 6 indicates N as a function of d for the droplets detected. Two peaks are seen at $d = 4.7$, 6.0 mm in the region of $4.2 < d < 6.5$ mm. The big droplets were mainly formed at the outlet of the oil injection tube located at (0, 0.25D, 2.4D). The direction of the lift force was downward (See Fig. 7), which was opposite to the buoyancy force at this location so that the net force acting on the oil was not stronger than the interfacial force. Thus, the oil clung to the outlet for long period due to the interfacial tension. The small droplets were formed at the outlet of the tube located at (0, -0.25D, 2.4D) where the direction of the lift force was the same as that of the buoyancy force so that the oil left the outlet quickly.

Axial Mean Velocity

The profile of axial mean velocity on the plane of $x = 0$ in the case with the droplets and that in the case without the droplets are compared in Fig. 8. The defect of the velocity is seen in the central region. This is due to the wake flow of the boss of the impeller. The difference in the profiles between the two cases is within the margin of error. This result is not the same as that in our previous study. Since the gradient of the V_z in the present study is higher than that in our previous study, the droplet motion towards the axis due to the lift force is more noticeable in the present study. The droplets moved to the axial direction have higher velocity than that of ambient fluid. This high velocity can be cancelled by the low velocity of wake flow by the droplets, which was originated at the detachment instant of the droplets from the tube outlets.

Turbulence Intensity in the Axial Direction

Figure 9 demonstrates the turbulence intensity in the axial direction in the case with the droplets and that without the droplets. The intensity in the case with the droplets is found to be higher than that without the droplets in the region of $-0.54 < 2y/D < 0.48$ except for the region of $0.13 < 2y/D < 0.22$. This exceptional region corresponds to that of N in Fig. 5. Thus, the enhancement of turbulence is the direct effect of the droplets. The increase in the intensity in the region of $-0.5 < 2y/D < 0$ is more noticeable than the other region. In this region, the direction of the droplet motion due to the lift force is upward and is the same as that of the rising velocity of the droplets due to the buoyancy (See Fig. 7). Thus, the relative motion of the droplets to the ambient fluid was intensified by the lift force and the buoyancy force. For some typical droplets, the Reynolds number based on the instantaneous relative velocity between the droplet and the surrounding flow v_{rel}, the droplet diameter d and ν, $Re_d = v_{rel}d/\nu$, was approximately equal to 150. According to the experimental result of flow around the sphere carried out by Sakamoto and Haniu (1990), faint periodic pulsative motion occurs for a very long period at the rear of the vortex-ring from behind the sphere in the case where Re_d is in the range of 130 − 300. Thus, it can be considered that similar periodic pulsative motion is generated in the wake region of the droplets. This motion causes an increase in the intensity.

CONCLUSIONS

We carried out the measurement on the turbulent swirling water flow with the immiscible oil droplets in a horizontal pipe. The main conclusions obtained are as follows:

(1) The droplet distribution had the twin-peak distribution. The big droplets were generated by the long-term clinging of oil at the outlet of the oil injection tube. This is due to the force balance associated with the water swirl motion and the buoyancy.

(2) The low-density droplets in the central region moved in the axial direction due to the lift force and buoyancy force. These droplets had higher velocity than the ambient water and the wake flow of the droplets had lower velocity than the ambient water. Thus, the axial mean velocity of the water flow was not affected by the droplets.

(3) It is expected that the faint periodic pulsative motion occurs for a very long period at the rear of the vortex-ring from behind some droplets. This motion caused the increase in the axial turbulence intensity.

REFERENCES

Etoh, T., Takehara, K., and Okamoto, K., 1999, “Performance Evaluation of the PMC and the KC Methods for Particle Extraction and Tracking through Their Application to Standard Particle Images (in Japanese)”, *Trans. Japan Soc. Mech. Eng. Ser B*., Vol. 65, pp.1688 − 1695.

Hagiwara, Y., Suzaki, T., and Saegusa, D., 2005, “Interaction between Near-wall Turbulence Structure and Immiscible Droplets Falling with Wobbling Motion in Upward Water Flow”, *Energy*, Vol. 30, pp. 181 − 195.

Hagiwara, Y. Yuge, T., and Takagaki, S., 2003, “Effects of a Droplet on Near-wall Transport Phenomena in Turbulent Downward Liquid-liquid Flow”, *Journal of Enhanced Heat Transfer*, Vol.10, pp.103 − 115.

Hjelmfelt Jr, A. T., and Mockros, L. F., 1966, “Motion of Discrete Particles in a Turbulent Fluid”, *Applied Scientific Research,* Vol.16, pp.149 − 161.

Inaba, H., Horibe, A., Ozaki, K., and Yokoyama, N., 1998, “Liquid-liquid Direct Contact Heat Exchange Using a Perfluorocarbon Liquid for Waste Heat Recovery (Heat Transfer Characteristics Obtained with Perfluorocarbon Droplets Descending in a Hot Water Medium) (in Japanese)”, *Trans. Japan Soc. Mech. Eng. Ser B.,* Vol. 64, pp. 3838 − 3845.

Ishikawa, M., Murai, Y., Wada, A. Iguchi, M. Okamoto, K., and Yamamoto, F., 2000, “A Novel Algorithm for Particle Tracking Velocimetry Using the Velocity Gradient Tensor”, *Experiments in Fluids*, Vol.29, pp.519 − 531.

Jacobs, H. R., and Golafshani, M., 1989, "A Heuristic Evaluation of the Governing Mode of Heat Transfer in a Liquid-liquid Spray Column", *ASME Journal of Heat Transfer*, Vol.111, pp. 773 − 778.

Kaviany, M., 1994, *Principles of Convective Heat Transfer*, Springer-Verlag, New York.

Kitoh, O., 1991, "Experimental study of turbulent swirling flow in a straight pipe", *Journal of Fluid Mechanics*, Vol.225, pp.445 − 479.

Kouda, T., and Hagiwara, Y., 2005, "Turbulent Swirling Water Flow with Oil Droplets", *Multiphase Science and Technology*, Vol. 17, (accepted).

Lee, J. M., 1987, "Drop Size Formations in Agitating System", *Encyclopedia of Fluid Mechanics* (ed. by N. P. Cheremisinoff), Vol. 6, Chapter 5, Gulf Pub. Co., Houston.

Magaud, F., Nijafi, A. F., Angilella, J. R., and Souhar, M., 2003, "Modeling and Qualitative Experiments on Swirling Bubbly Flows: Single Bubble with Rossby Number of Order 1", *ASME Journal of Fluids Engineering*, Vol.125, pp.239 − 246.

Mitrovic, J., and Stephan, K., 1996, "Mean Fluid Temperatures in Direct Contact Heat Exchangers without Phase Change", *Int. Journal of Heat and Mass Transfer*, Vol. 39, pp. 2745 − 2750.

Okamoto K. et al., 2002, *Handbook of Particle Image Velocimetry* (ed. the Visualization Society of Japan) (in Japanese), Chapter 4, Morikita Pub. Co., Tokyo.

Sakamoto, H., and Haniu, H., 1990, "A study on vortex shedding from spheres in a uniform flow", *ASME Journal of Fluids Engineering*, Vol. 112, pp. 386 − 392.

Satake, S., and Kunugi, T., 1998, "Direct Numerical Simulation of Turbulent Pipe Flow (in Japanese)", *Trans. Japan Soc. Mech. Eng. Ser B.*, Vol. 64, pp. 65 − 70.

Tanaka, Y., Oba, G., and Hagiwara, Y., 2003, "Experimental Study on the Interaction between Large Scale Vortices and Particles in Liquid-solid Two-phase Flow", *Int. Journal of Multiphase Flow*, Vol.29, pp.361 − 373.

Table 1: Physical properties.

	Water	KF995
Specific weight [-]	1	0.96
Kinematic viscosity [mm^2/s]	1.0	4.0
Surface tension [mN/m]	-	17.8
Refractive index [-]	1.33	1.40

Table 2: Image-capturing conditions.

	(x, y)-plane	(y, z)-plane
Capturing rate [frame/s]	48	95
Pixel numbers	1004 × 1004	1000 × 248
Pixel resolution [mm^2]	0.050 × 0.050	0.059 × 0.059
Frame numbers per run	7800	12800

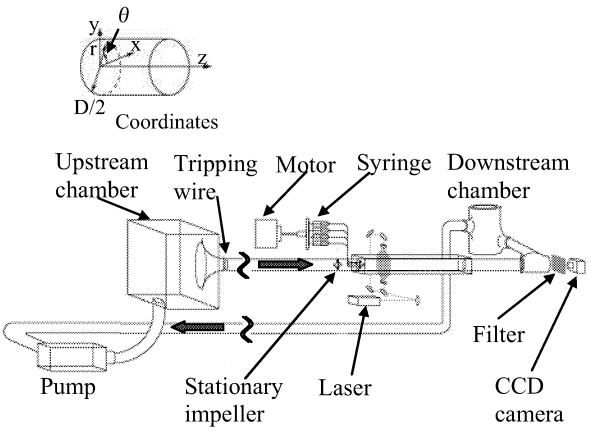

Figure 1 Schematic diagram of apparatus.

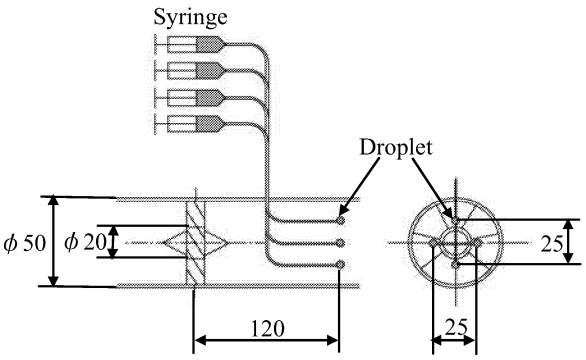

Figure 2 Details of impeller and droplet injection tubes. Dimensions in mm.

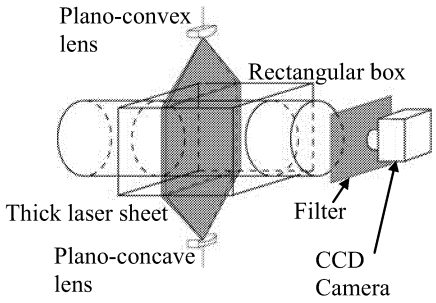

(a) Axial view

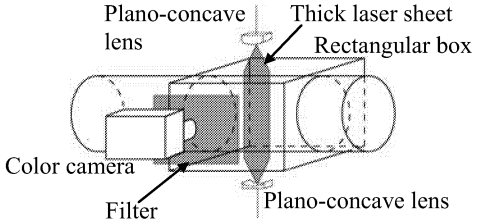

(b) Side view

Figure 3 Arrangement of optics and cameras.

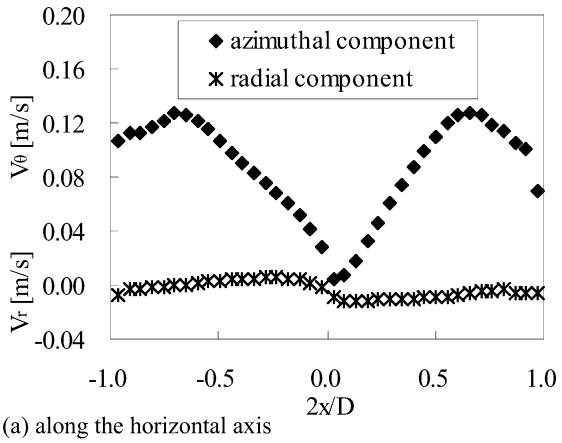

(a) along the horizontal axis

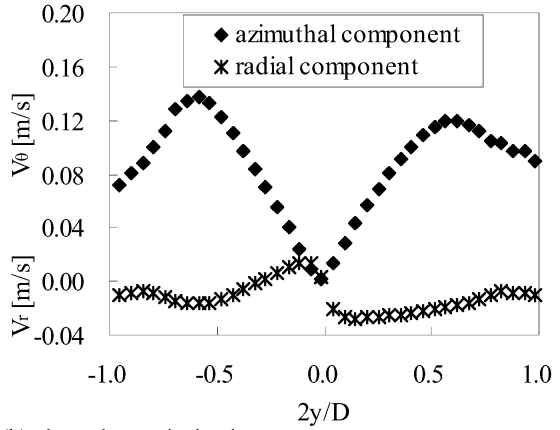

(b) along the vertical axis

Figure 4 Mean velocities in the azimuthal and radial directions.

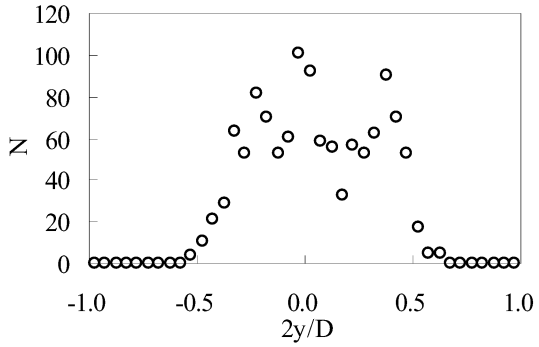

Figure 5 Number of frames with droplet images.

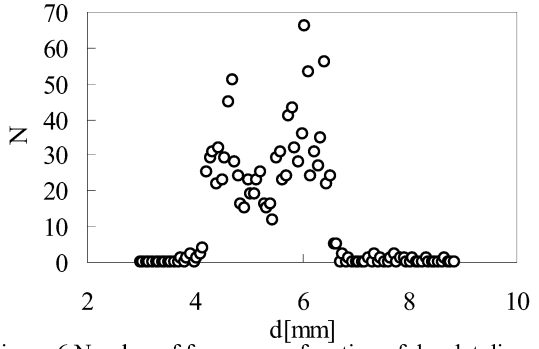

Figure 6 Number of frames as a function of droplet diameter.

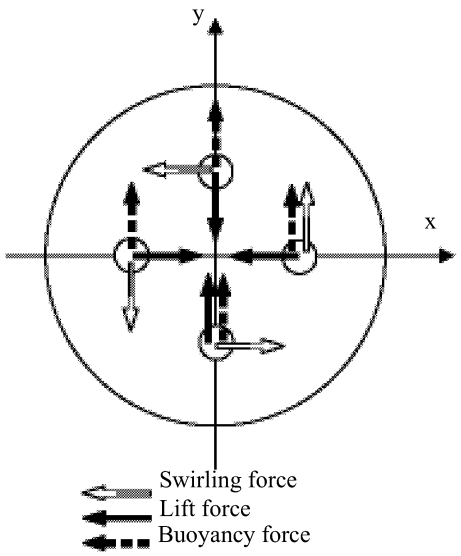

Figure 7 Forces acting on droplets

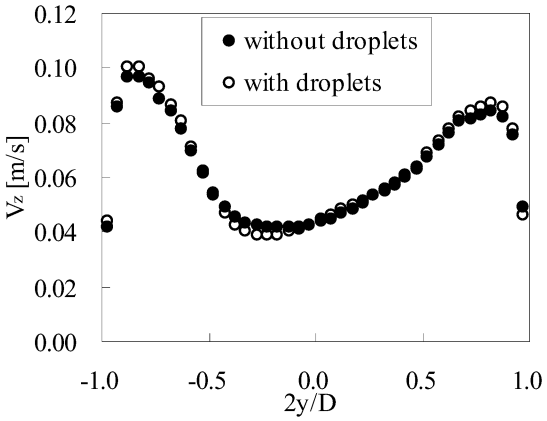

Figure 8 Profiles of axial mean velocity.

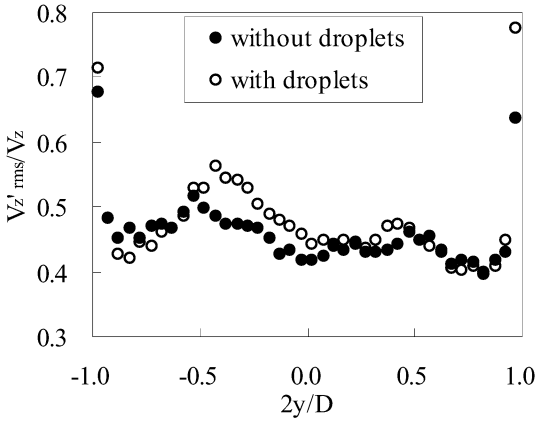

Figure 9 Turbulence intensity in the axial direction.